High speed friction stir welding of aluminium alloys

D. M. Rodrigues*[1], C. Leitão[1], R. Louro[2], H. Gouveia[2] and A. Loureiro[1]

In this paper, the weldability of AA 5083-H111 (non-heat treatable) and AA 6082-T6 (heat treatable) aluminium alloys, which are widely used in welding fabrication, is compared by analysing the welds obtained from both materials under a large range of welding conditions (varying tool dimensions, rotation and traverse speeds, axial loads and tilt angles) chosen to ensure high welding speeds. The differences in friction stir weldability, assessed by weld defect analysis and weld strength characterisation, will be related to the markedly different plastic behaviours of both base materials. Based on the experimental results, a methodology for determining suitable friction stir welding parameters is proposed.

Keywords: Aluminium, Weldability, Productivity, Process parameters, Plasticity

Introduction

The friction stir welding (FSW) process is commonly accepted as a promising method for joining light metallic alloys. However, the extended application of this welding process in industry still requires accurate knowledge of the joining mechanism, and the metallurgical and mechanical transformations it induces in the base materials. This knowledge will then allow the establishment of suitable welding parameters for joining a large range of materials in varied weld configurations, such as different plate thicknesses or joint types. Another important aspect is to guarantee improved levels of welding productivity. Since the welding speed has a direct influence on the process productivity,[1] in any welding operation in an industrial context, the objective behind the selection of suitable welding parameters has to be to maximise the welding speed while ensuring acceptable welding quality.

Although FSW technology has attracted significant interest from the aerospace and transportation industries, and extensive literature exists on FSW, there are few reported systematic studies on process parameter optimisation. Example of this is the extensive literature published concerning the joining of aluminium alloys, for which a deep revision can be found in Refs. 2–4 and examples of very recent works already performed in magnesium,[5] copper,[6] steel[7] and titanium.[8] On the other hand, though numerical modelling of plastic flow in FSW has provided guidelines concerning tool design and weld quality optimisation,[9] there does not appear to have been an application of these models towards the prediction of practical processing maps. The only principle globally accepted is that, for each set of welding conditions (joint type, base material and plate thickness), a specific set of welding parameters must be used to ensure acceptable process behaviour.

In this paper, the weldabilities in FSW of AA 5083-H111 (non-heat treatable) and AA 6082-T6 (heat treatable) aluminium alloys, which are widely used in welding fabrication, are compared by analysing the welds obtained from both materials under a large range of welding conditions (varying tool dimensions, rotation speeds, axial loads and tilt angles) and high welding speeds. The differences in friction stir weldability, which were evaluated based on weld defect analysis and weld strength characterisation, are related to the different mechanical and microstructural evolutions with temperature and plastic deformation of the base materials. These differences lead to drastically different welding behaviours, as has already been described in previous studies.[11–24] In fact, among the base materials already joined by FSW, the 6xxx series of aluminium alloys is the most widely analysed under a large range of welding conditions. According to these previous studies, the mechanical properties of the AA 6xxx friction stir welds depend mainly on the size, volume fraction and distribution of precipitates in the weld line and adjacent heat affected zone (HAZ). Friction stir welding of the non-heat treatable aluminium alloys, such as the AA 5xxx series, is much less studied than for the AA 6xxx alloys. However, it has already been established that the mechanical properties of the welds produced from the AA 5xxx alloys depend mainly on the grain size and on the density of the dislocations after plastic deformation and recrystallisation occurring during welding. When the AA 5xxx alloy series is used under the annealed condition, the microstructure is stable and usually no softening occurs in the weld zone and HAZ. In contrast, when these alloys are used under the strain hardened condition, the work hardened structure will readily recover and/or recrystallise during welding, and softening may occur.
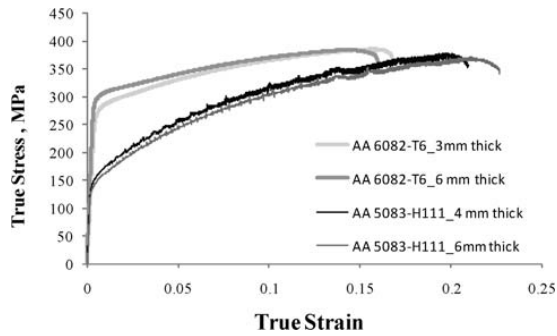
1 Base materials tensile stress–strain curves

COLOUR
FIGURE
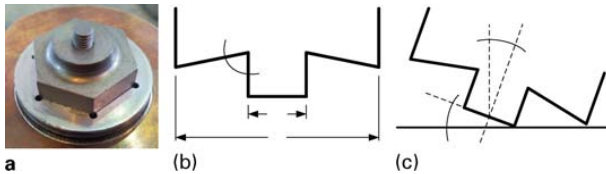
2 *a* friction stir welding tool and *b*, *c* sketches of tool geometry

Experimental

Base materials

In the current investigation, two aluminium alloys widely used in welding fabrication were studied, namely, the AA 5083-H111 (non-heat treatable) aluminium alloy, supplied in plates of 4 and 6 mm thickness, and the AA 6082-T6 (heat treatable) aluminium alloy, supplied in plates of 3 and 6 mm thickness. These base materials have markedly different mechanical behaviours, as exemplified in Fig. 1, where their corresponding tensile stress–strain curves are shown. From these curves it is possible to conclude that, for each base material, the mechanical properties are consistent although they were supplied in plates of different thicknesses, and so were from different batches. If the curves plotted in Fig. 1 are compared, it is possible to conclude that the AA 5083-H111 alloy, with 148 MPa yield strength, is much softer than the AA 6082-T6 alloy, with 290 MPa yield strength. However, despite being softer, the AA 5083-H111 exhibits strong Portevin–Le Châtelier effect and pronounced hardening with plastic deformation, attaining tensile strength values close to that of the AA 6082-T6 alloy. This pronounced difference in plastic deformation behaviour will naturally influence the FSW weldability of both types of alloys.

Welding procedure

Friction stir welds were performed in 4 and 6 mm thick sheets of the AA 5083-H111 alloy (5_4 and 5_6 respectively) and 3 and 6 mm thick sheets of the AA 6082-T6 alloy (6_3 and 6_6 respectively), under a large range of welding conditions, using a conical shoulder tool with a cylindrical threaded pin (Fig. 2). Although the geometry was maintained, tool dimensions, especially the pin diameter D_p and shoulder diameter D_s, were varied according to the plate thickness to be welded, as shown in Table 1. The pin length was set so as to guarantee that during the welding operation the lowermost surface of the pin did not come in contact with the backing bar but was never more than 0·1 mm away from it. Bead on plate welds were produced for the four different types of plates. This procedure enabled to eliminate the influence of sheet positioning and clamping on the resulting weld quality.

For the different types of tools tested in this study, the welding speed v, rotation speed w and vertical force F_z were varied, as shown in Table 2, and also the tilt angle α, as shown in Table 1. The process parameter values were selected based on bibliographic references, the capability of the available equipment and the past experience of the working group. Figure 3 shows a graph which summarises the rotation and traverse speeds (maximum values) used by other authors to perform friction stir welds in the base materials under study, and also the w–v windows considered in the current investigation for each base material and plate thickness. As shown in the graph, the maximum traverse speeds tested in the present work were always higher than those in previous studies. From Table 2 and Fig. 3 it is possible to see that for the 6 mm thick plates, similar welding parameters were established to highlight the differences in weldability between the two base materials. Testing plans were established by combining the different tool and processing parameters for each plate thickness and base material, determining a total of 144 welds to be performed. For example, the testing plan for the 6_3 plates is shown in Fig. 4.

Testing procedure

After welding, all the sheets were visually inspected for surface defects like excessive flash and surface flaws.

Table 1 Tool parameters

Plate type	Shoulder diameter D_s, mm				Pin diameter D_p, mm		Tilt angle α, °		
6_3	10	12	13	15	4	5	1	2	3
5_4	13		15	18	5	6	1	2	3
6_6	15		18	21	6	7	1	2	3
5_6	15		18	21	6	7	1	2	3

Table 2 Process parameters

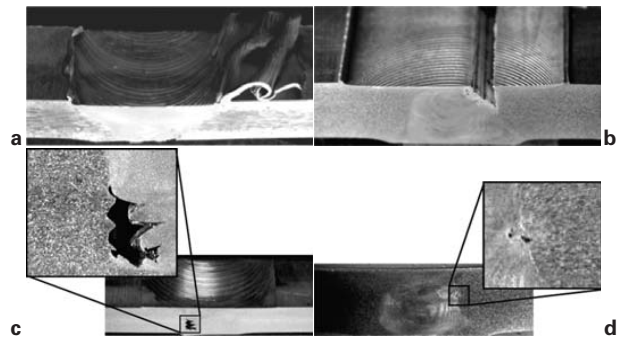| Plate type	Welding speed v, mm min^{-1}			Rotation speed w, rev min^{-1}			Vertical force F_z, kN		
6_3	800	950	1100	1000	1150	1300	5	7	9
5_4	300	400	500	400	500	600	7	11	15
6_6	200	275	350	300	400	500	10	15	20
5_6	200	275	350	300	400	500	10	15	20
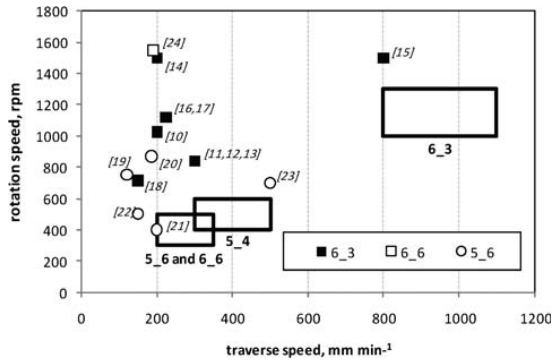
3 Rotation and traverse speeds used for friction stir welding of AA 5083 and AA 6082 alloys

Transverse specimens for metallographic analysis and hardness testing were cut from the welds with no important surface defects, using water jet cutting. For the metallographic analysis, the transverse sections of the welds were cold mounted, polished and etched with Poulton's modified reagent, and observed using Zeiss Axiotech 100 HD and Zeiss Stemi 2000-C microscopes, for detecting large and very small internal flaws respectively. The heterogeneity in mechanical properties across the welds with slight or no defects was evaluated by performing hardness measurements transversely to the weld direction, using a Shimadzu microhardness tester with 200 gf load for 15 s. Tensile tests were also performed, all of which were carried out at room temperature at a crosshead speed of 5 mm min^{-1} using an Instron computer controlled testing machine. Tensile properties were evaluated by testing three tensile specimens of each type. The tensile samples were not machined in order to eliminate weld surface roughness and its possible influence on the plastic behaviour of the samples. During testing, the global performance of the welded plates was evaluated by using a mechanical extensometer of 50 mm gauge length. The local plastic behaviour of the thermomechanically affected zone and HAZ was also analysed using optical strain data acquisition.

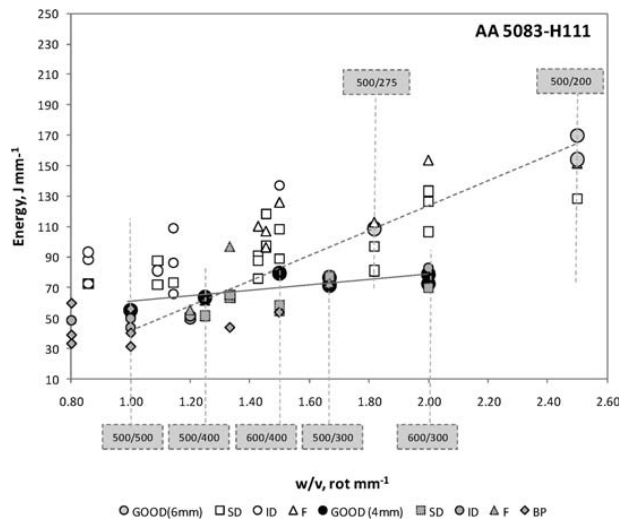*a* flash (F); *b* surface defect (SD); *c* internal defect (ID); *d* very small defect

**5 Tipical welding defects**

Results

Visual inspection

As mentioned above, qualitative inspection of the welds was performed by visual examination to detect surface defects, followed by metallographic analysis to detect internal flaws. This inspection detected three basic types of defects: excessive flash (F) (Fig. 5a), surface flaws (SD) (Fig. 5b) and internal voids (ID) (Fig. 5c). Under some welding conditions, the pin was broken (BP) and it was not possible to perform the weld. These situations have also been indicated.

The energy E (in J mm^{-1}) consumed per unit length of weld, for all the weld tests, was determined by dividing the average power P by the welding velocity ($E=P/v$). The average power was obtained by multiplying the torque T, registered from the welding machine during the welding operation, by the rotation speed ($P=Tw$). Figures 6 and 7 plot the energy consumed per unit length of weld versus the ratio w/v for the 5083 and 6082 welds respectively. In the graphs, the results are grouped according to the classification of the welds after visual inspection. The results identified as GOOD comprise both the non-defective welds and the welds with very small defects (e.g. Fig. 5d) that were considered unimportant for the global strength of the weld. If the results from the graphs are compared, it is possible to conclude that for the range of welding parameters

	D_p [mm]	D_s [mm]	a [°]	v [mm/min]	w [RPM]	F_z [kN]
1	4	10	1	800	1000	5
2	4	10	2	800	1150	7
3	4	10	3	800	1300	9
4	4	12	1	800	1000	5
5	4	12	2	800	1150	7
6	4	12	3	800	1300	9
7	5	13	1	800	1000	7
8	5	13	2	800	1150	9
9	5	13	3	800	1300	5
10	5	15	1	800	1000	9
11	5	15	2	800	1150	5
12	5	15	3	800	1300	7
13	4	10	1	950	1150	9
14	4	10	2	950	1300	5
15	4	10	3	950	1000	7
16	4	12	1	950	1150	9
17	4	12	2	950	1300	5
18	4	12	3	950	1000	7
19	5	13	1	950	1150	5
20	5	13	2	950	1300	7
21	5	13	3	950	1000	9
22	5	15	1	950	1150	7
23	5	15	2	950	1300	9
24	5	15	3	950	1000	5
25	4	10	1	1100	1300	7
26	4	10	2	1100	1000	9
27	4	10	3	1100	1150	5
28	4	12	1	1100	1300	7
29	4	12	2	1100	1000	9
30	4	12	3	1100	1150	5
31	5	13	1	1100	1300	9
32	5	13	2	1100	1000	5
33	5	13	3	1100	1150	7
34	5	15	1	1100	1300	5
35	5	15	2	1100	1000	7
36	5	15	3	1100	1150	9

4 Welding plan for 6_3 plates

6 Energy consumed per unit length of weld versus w/v, for AA 5083-H1114 welds (4 and 6 mm thick plates)
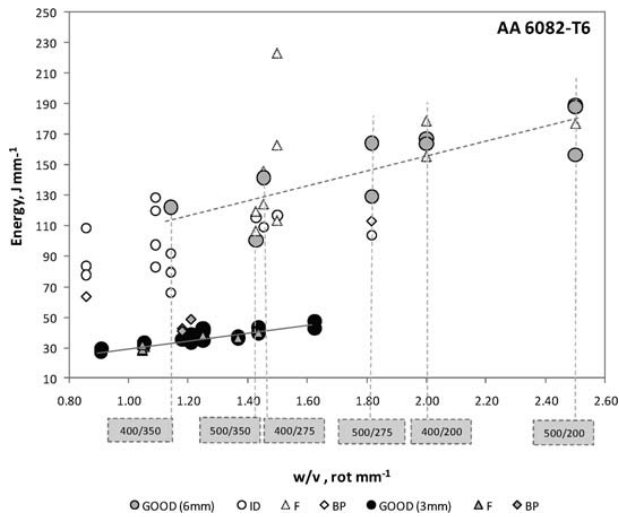
7 Energy consumed per unit length of weld versus *w/v* for AA 6016-T6 welds (4 and 6 mm thick plates)

tested in this study the 6082 aluminium alloy presents higher weldability than the 5083 alloy, since a large number of acceptable welds (good and small defect welds) were obtained for both plate thicknesses. However, it is important to remark that the number of non-acceptable welds (F, SD, ID and BP) was very high for all the alloys and plate thicknesses, showing that the process is very sensitive to the choice of tool and machine parameters.

A more detailed analysis of the welding results presented in Figs. 6 and 7 enabled some unacceptable welding parameters for each type of plate to be determined. These are identified in Tables 1 and 2 by colouring the cells grey. A welding parameter was considered unacceptable when all the welds produced under welding conditions including this parameter (α, D_p, D_s, v, w or F_z) were defective. For the 5_4 plates, parameters leading to only one good weld were also considered unacceptable. Analysing the grey cells in Table 1, it can be seen that no acceptable welds were produced with the narrower shoulders in any of the plates. At the same time, qualitative analysis revealed that the process was relatively unaffected by changing pin dimensions. For both alloys, the main defect that could be directly related to the small shoulder diameter was flash formation. A very small tool tilt angle ($\alpha=1°$) also led to flash formation, especially for the thicker plates. For the 5_4 plates, the 18 mm shoulder tool was also found wanting, since it only produced one good weld. However, in this case no specific defect type could be related to shoulder size.

Another important limiting factor for successful welding was the choice of the axial load (*see* grey cells in Table 2). However, the sensitivity of the welds to this parameter is highly influenced by the nature of the base material. In fact, for the 5083 alloy, it was found that using very low axial loads (7 and 11 kN, for the 4 mm thick plate, and 10 kN, for the 6 mm plate) led to significant superficial and internal welding defects, which indicates that these values are the lower axial load limits for FSW of these plates. On the other hand, for the 6082 alloy, no clear limit for axial load was found when welding the 6 mm thick plates. For the 3 mm plates, a maximum load of 9 kN was determined, since

the pin was destroyed in all tests performed with this axial load. Finally, for the 5083 alloy, serious limitations in rotation speed (400 rev min^{-1} for the 4 mm thick plates, and 300 and 400 rev min^{-1} for the 6 mm thick plates) and traverse speed (500 mm min^{-1} for the 4 mm thick plates and 350 mm min^{-1} for the 6 mm thick plates) were also registered. Low rotation speeds and high traverse speeds led to the formation of large internal defects, and for the 5_4 plates, they were also associated with tool destruction (BP) in many cases. Large internal defects also occurred for the 6082 alloy in 6 mm thick plates, for the low rotation speed of 300 rev min^{-1}. Previous authors[25] have already associated the formation of internal and surface defects with insufficient heat input, which in turn is usually related to low rotation speeds and high traverse speeds as in the current study.

Looking carefully at the results presented in Fig. 6, for the 5_6 plates, it is possible to conclude that only three GOOD welds were obtained for these plates. There were a large number of welds with internal and surface defects and also two situations in which the pin was broken. Globally the energy results are widely dispersed and it was impossible to establish any relationship between the energy consumed in the process and the process parameters. However, if only the GOOD weld energy values are considered (large grey circles), which presumably correspond to equilibrium welding conditions, a linear regression can be used to fit the results, which indicate that the energy consumed in the process increases with increasing *w/v* ratios. For the 5_4 plates, more non-defective welds were achieved under the selected welding conditions. For these plates, the energy consumed in the process was lower than that for the 5_6 welds and the results are much less dispersed, indicating weld conditions closer to equilibrium. This can be also inferred by fitting the results relative to the GOOD welds. These results show that the energy increases almost linearly with *w/v*, but at a much lower rate than that for the 5_6 welds.

In analysing the results from the 6082 alloy (Fig. 7), it is possible to see that with this base material the principal defect types were: flash formation, for both plate thicknesses, caused by inappropriate shoulder dimensions; internal defects, for the 6_6 plates, brought about by low tool rotation speed; and a large number of broken pin situations for the 6_3 plate, caused by excessive axial loads. Just as for the 5083 alloy, the energy values for the GOOD welds can be fitted using linear interpolation, indicating increasing values with increasing *w/v* ratios. For the 6_3 plates, the energy consumed is almost the same for both defective and GOOD welds, which indicates that at higher rotation speeds, which will correspond to hotter welding conditions, the process becomes very stable. On the other hand, for the 6_6 plates, energy results are more widely dispersed, especially for low *w/v* ratios and/or $w=300$ rev min^{-1}, which correspond to colder welding conditions. As the rotation speed increases (6_3 plates), the energy consumed in the process becomes less dependent on process parameters, and is similar for both GOOD and defective welds.

Mechanical testing results

The mechanical efficiency of the GOOD welds was analysed by calculating yield strength efficiency coefficient
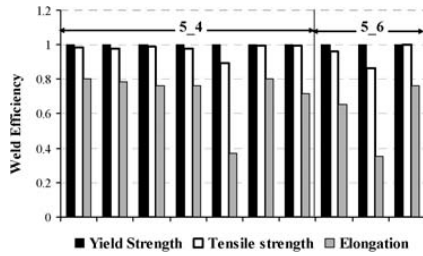
8 Mechanical efficiencies for 5_6 and 5_4 welds

■ Yield Strength ☐ Tensile strength ▨ Elongation

1 η_{ys} and tensile strength efficiency coefficient η_{Rm} respectively, defined as the ratio between the yield or tensile strength of the transverse weld samples (considering a 50 mm gauge length) and the same properties of the parent materials. An elongation coefficient η_e, which is the ratio between the elongation of the weld samples and base materials at maximum load, was also calculated. The results obtained for the 5083 and 6082 welds are summarised in Figs. 8 and 9. As shown in Fig. 8, the 5_6 and 5_4 welds are almost in yield and tensile strength even match ($\eta_{Rm}=1$ and $\eta_{ys}=1$) relative to the parent plates, except in two situations where the welds had very small defects. However, even for these small defect welds the tensile strength efficiency is almost 85%. Despite the good strength of the welds, its elongation is lower than that of the base plates, never exceeding 80% efficiency and falling to 35% for the small defect welds. This behaviour is a result of slight overmatch conditions of weld material relative to base material, as exemplified in Fig. 10. This shows local tensile stress–strain curves for the welds and parent plates from the tensile tests of 5_4 and 5_6 transverse samples, and the hardness profiles across the same welds (it is important to point out that in order to plot the two different types of results on the same graph, the logarithm strain values were multiplied by 100 as indicated above the *x* axis). The figure also shows the longitudinal strain distribution, after maximum load, for both samples. It is possible to see that necking occurred in the base material, for the 5_6 sample, and in the weld, for the 5_4 sample, which actually corresponded to a small defect sample. Actually, the two welds were deformed but to a lower extent than the base material, which led to lower global elongation levels for the transverse welded samples, even for the non-defective welds. The stress–strain curves of the welds and their hardness profiles confirm the slight overmatch behaviour of the welds. It is important to highlight that very similar mechanical performance was registered for all the GOOD welds although they were obtained using different process parameters.

Turning to the mechanical efficiency results for the 6082 alloy, plotted in Fig. 9, it is possible to conclude
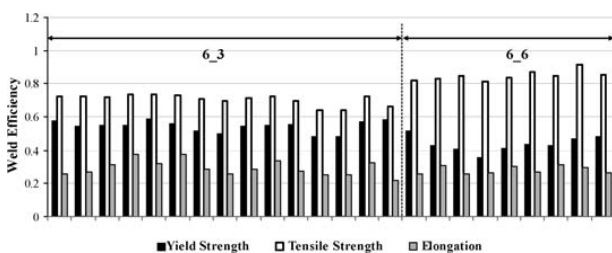

9 Mechanical efficiencies for 6_6 and 6_3 welds

■ Yield Strength ☐ Tensile Strength ▨ Elongation

COLOUR FIGURE
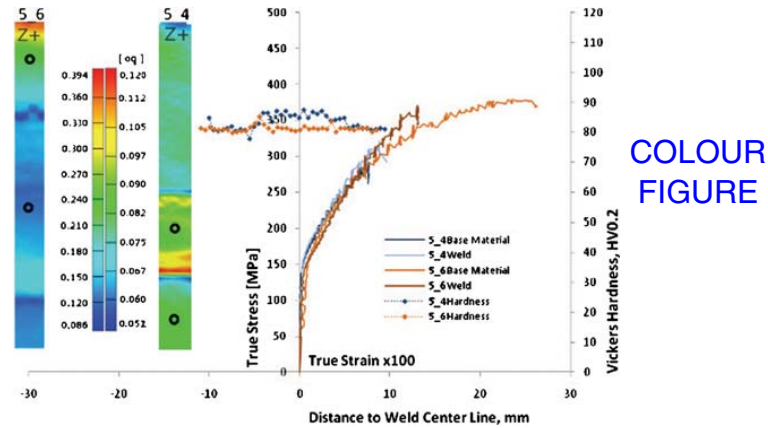
10 Hardness and tensile test results for 5_4 ($w=600$ rev min^{-1}, $v=400$ mm min^{-1}, $D_s=18$ mm, $F_z=15$ kN) and 5_6 ($w=500$ rev min^{-1}, $v=250$ mm min^{-1}, $D_s=21$ mm, $F_z=20$ kN) weld samples: small circles in sample images indicate location of points for which stress–strain curves were plotted

that all the 6_3 and 6_6 welds were in undermatch relative to the base material since the weld efficiency was always <1. However, although a slightly higher yield stress undermatch was registered for the 6_6 welds (averaging 60%) than for the 6_3 welds (averaging 50%), the 6_6 welds displayed slightly higher tensile strengths. The average elongation efficiency is similar for both weld types, averaging 30%. These results can be understood by analysing the curves in Fig. 11, where the same type of results of Fig. 10 are plotted for the 6_3 and 6_6 welds. From the graph it is possible to see that both tensile samples failed in the weld, where the material is in undermatch condition relative to the base material, as confirmed by the low hardness values registered in the welds. Significantly, in the HAZ, the 6_6 weld exhibits lower hardness values than the 6_3 weld, which led to lower yield stress efficiencies for these welds. Since the maximum load was attained in the welds without plastic deformation of the base material, the corresponding tensile stress–strain curves are not presented in Fig. 11. It is also important to note that the 6_3 curve indicates greater strength than that of the 6_6 weld, which is in

COLOUR FIGURE
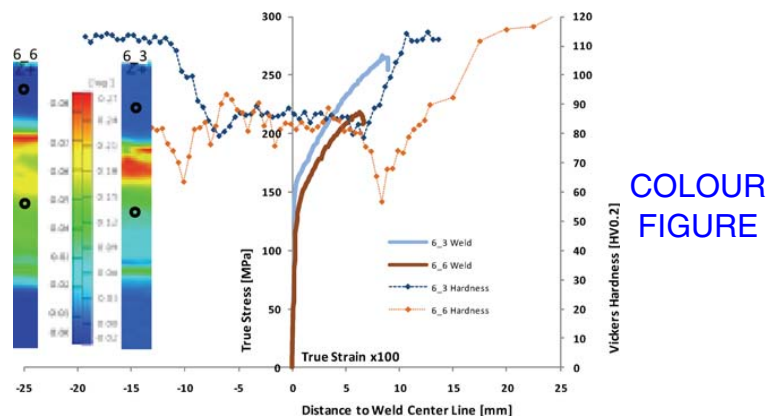
11 Hardness and tensile test results for 6_3 ($w=1300$ rev min^{-1}, $v=1100$ mm min^{-1}, $D_s=15$ mm, $F_z=5$ kN) and 6_6 ($w=400$ rev min^{-1}, $v=200$ mm min^{-1}, $D_s=18$ mm, $F_z=15$ kN) welds: small circles in sample images indicate location of points for which stress–strain curves were plotted

disagreement with the results shown in Fig. 9. Since the tensile tests (results in Fig. 11) were performed several months after the tests used to calculate the mechanical efficiency, it is reasonable to assume that natural age hardening of the weld material occurred.

Conclusions

From the above results it can be concluded that high traverse speeds can be achieved in FSW of both base materials with carefully chosen process and tool parameters. These in turn are strongly dependent on the base material characteristics and plate thickness. In fact the study proves that below certain shoulder dimensions dependent on plate thickness, and for very low tool tilt angles, it is not possible to achieve non-defective welds whatever the process parameters in use. In order to guarantee hot weld conditions an accurate selection of tool rotation speed is also very important. In fact, the calculation of the energy consumed in the process, as well as the analysis of the welds, shows that the process becomes relatively less dependent on process and tool parameters for high tool rotation rates. However, hot weld conditions are intimately related to the characteristics of the base material, and are far more easily attained for the harder 6082 alloy, to which higher values of plastic dissipation can be associated. The present study also shows that the establishment of accurate axial load values is also intimately related to the process parameters in use. Therefore, for cold weld conditions low axial loads led to significant internal and surface defects, whereas for hot weld conditions high axial load values led to tool destruction due to excessive plunge depth in the softened material. It was also shown that establishing suitable axial load values depends strongly on base material characteristics being advisable to perform tests in position control to determine appropriate axial load values. Finally, it was determined that the mechanical properties of the non-defective welds are relatively independent of the welding conditions. In the special case of the 6082 alloy, the use of very high welding speeds proved to be very effective in avoiding extra softening in the HAZ, with positive consequences in weld yield strength efficiency.

Acknowledgement

References

1. J. Mononen, M. Sirén and H. Hänninen: 'Cost comparison of FSW and MIG welded aluminium panels', *Weld. World*, 2003, **47**, 32–35.
2. D. M. Rodrigues, A. Loureiro, C. Leitão, R. M. Leal, B. M. Chaparro and P. Vilaça: 'Influence of FSW parameters on the microstructural and mechanical properties of AA 6016-T4 thin welds', *Mater. Des.*, 2009, **30**, 1913–1921.
3. C. Leitao, R. M. Leal, D. M. Rodrigues, A. Loureiro and P. Vilaça: 'Mechanical behaviour of similar and dissimilar AA 5182-H111 and AA 6016-T4 thin friction stir welds', *Mater. Des.*, 2009, **30**, 101–108.
4. R. S. Mishra and Z. Y. Ma: 'Friction stir welding and processing', *Mater. Sci. Eng. R*, 2005, **R50**, 1–78.
5. G. Padmanaban and V. Balasubramanian: 'Selection of FSW tool pin profile, shoulder diameter and material for joining AZ31B magnesium alloy – an experimental approach', *Mater. Des.*, 2009, **30**, (7), 2647–2656.
6. H. J. Liu, J. J. Shen, Y. X. Huang, L. Y. Kuang, C. Liu and C. Li: 'Effect of tool rotation rate on microstructure and mechanical properties of friction stir welded copper', *Sci. Technol. Weld. Join.*, 2009, **14**, (6), 577–583.
7. H. K. D. H. Bhadeshia and T. DebRoy: 'Critical assessment: friction stir welding of steels', *Sci. Technol. Weld. Join.*, 2009, **14**, (3), 193–196.
8. Y. Zhang, Y. S. Sato, H. Kokawa, S. H. C. Park and S. Hirano: 'Microstructural characteristics and mechanical properties of Ti–6Al–4V friction stir welds', *Mater. Sci. Eng. A*, 2008, **A485**, (1–2), 448–455.
9. R. Nandan, T. DebRoy and H. K. D. H. Bhadeshia: 'Recent advances in friction stir welding – process, weldment, structure and properties', *Prog. Mater. Sci.*, 2008, **53**, (6), 980–1023.
10. M. Barletta, G. Buffa, L. Casamichele and L. Fratini: 'Local mechanical and morphological characterization of friction stir-welded butt joints', *Proc. IMechE B*, 2006, **220B**, 813–821.
11. A. Steuwer, M. J. Peel and P. J. Withers: 'Dissimilar friction stir welds in AA5083–AA6082: the effect of process parameters on residual stress', *Mater. Sci. Eng. A*, 2006, **A441**, 187–196.
12. M. J. Peel, A. Steuwer, P. J. Withers, T. Dickerson, Q. Shi and H. Shercliff: 'Dissimilar friction stir welds in AA5083–AA6082. Part I: Process parameter effects on thermal history and weld properties', *Metall. Mater. Trans. A*, 2006, **37A**, (7), 2183–2193.
13. M. J. Peel, A. Steuwer and P. J. Withers: 'Dissimilar friction stir welds in AA5083–AA6082 Part II: Process parameter effects on microstructure', *Metall. Mater. Trans. A*, 2006, **37A**, (7), 2195–2206.
14. L. Fratini, G. Buffa, L. Filice and F. Gagliardi: 'Friction stir welding of AA6082-T6 T-joints: process engineering and performance measurement', *Proc. IMechE B*, 2006, **220B**, (5), 669–676.
15. P. M. G. P. Moreira, M. A. V. de Figueiredo and P. M. S. T. de Castro: 'Fatigue behaviour of FSW and MIG weldments for two aluminium alloys', *Theor. Appl. Fract. Mech.*, 2007, **48**, (2), 169–177.
16. P. M. G. P. Moreira, T. Santos, S. M. Tavares, V. Richter-Trummer, P. Vilaça and P. M. S. T. de Castro: 'Mechanical characterization of friction stir welds of two dissimilar aluminium alloys of the 6xxx series', *Mater. Sci. Forum*, 2008, **587–588**, 430–434.
17. P. M. G. P. Moreira, T. Santos, S. M. O. Tavares, V. Richter-Trummer, P. Vilaça and P. M. S. T. de Castro: 'Mechanical and metallurgical characterization of friction stir welding joints of AA6061-T6 with AA6082-T6', *Mater. Des.*, 2009, **30**, 180–187.
18. L. Fratini, G. Buffa and R. Shivpuri: 'Influence of material characteristics on plastomechanics of the FSW process for T-joints', *Mater. Des.*, 2009, **30**, 2435–2445.
19. P. A. Colegrove: '3-dimensional CFD modelling of flow round a threaded friction stir welding tool profile', *J. Mater. Process. Technol.*, 2005, **169**, 320–327.
20. H. Lombard, D. G. Hattingh, A. Steuwer and M. N. James: 'Optimising FSW process parameters to minimise defects and maximise fatigue life in 5083-H321 aluminium alloy', *Eng. Fract. Mech.*, 2008, **75**, 341–354.
21. G. R. Cui, Z. Y. Ma and S. X. Li: 'Periodical plastic flow pattern in friction stir processed Al–Mg alloy', *Scr. Mater.*, 2008, **58**, 1082–1085.
22. D. G. Hattingh, C. Blignault, T. I. van Niekerk and M. N. James: 'Characterization of the influences of FSW tool geometry on welding forces and weld tensile strength using an instrumented tool', *J. Mater. Process. Technol.*, 2008, **203**, 46–57.
23. G. R. Cui, Z. Y. Ma and S. X. Li: 'The origin of non-uniform microstructure and its effects on the mechanical properties of a friction stir processed Al–Mg alloy', *Scr. Mater.*, 2009, **57**, 5718–5729.
24. T. Minton and D. J. Mynors: 'Utilisation of engineering workshop equipment for friction stir welding', *J. Mater. Process. Technol.*, 2006, **177**, 336–339.
25. M. Iordachescu, D. Iordachescu, J. L. Ocana, P. Vilaça and E. Scitelnicu: 'Characteristic flaws in aluminium alloys joints', *Metal. Int.*, 2009, **12**, (2), 135.

Authors Queries

Dear Author
During the preparation of your manuscript for publication, the questions listed below have arisen. Please attend to these matters and return this form with your proof. Many thanks for your assistance

Query Reference	Query	Remarks
1	Author: Please confirm the meanings of η_{ys} and η_{Rm}.	
2	Author: Please cite reference 10 in the text.	